GA–A22226

THE SPHERICAL TOKAMAK PATH TO FUSION POWER

by
R.D. STAMBAUGH, V.S. CHAN, R.L. MILLER,
and M.J. SCHAFFER

MAY 1996

GA–A22226

THE SPHERICAL TOKAMAK PATH TO FUSION POWER

by
R.D. STAMBAUGH, V.S. CHAN, R.L. MILLER,
and M.J. SCHAFFER

This is a preprint of a paper to be submitted for publication in *Fusion Technology.*

GA PROJECT 4437
MAY 1996

ABSTRACT

The low aspect ratio tokamak or spherical torus (ST) approach offers the two key elements needed to enable magnetic confinement fusion to make the transition from a government-funded research program to the commercial marketplace: a low cost, low power, small size market entry vehicle and a strong economy of scale in larger devices. Within the ST concept, a very small device (A = 1.4, major radius about 1m, similar size to the DIII–D tokamak) could be built that would produce ~800 MW thermal, 250 MW net electric, and would have a gain, defined as Q_{PLANT} = (gross electric power/recirculating power), of about 2. Such a device would have all the operating systems and features of a power plant and would therefore be acceptable as a pilot plant, even though the cost of electricity would not be competitive. The ratio of fusion power to copper TF coil dissipation rises quickly with device size (like $R^3 – R^4$, depending on what is held constant) and can lead to 3 GW thermal power plants with Q_{PLANT} = 4–5 but which remain a factor 3 smaller than superconducting tokamak power plants. Power plants of the scale of ITER might be able to burn the advanced fuel D-He^3. These elements of a commercialization strategy are of particular importance to the U.S. fusion program in which any initial non-government financial participation demands a low cost entry vehicle.

The ability to pursue this line of fusion development requires certain advances and demonstrations which are probable. Stability calculations support a specific advantage of low aspect ratio in high beta which would allow simultaneously β_T ~ 60% and 90% bootstrap current fraction (I_p ~ 16 MA, κ = 3). Steady state current drive requirements are then manageable. The high beta capability means the fusion power density can be so

high that neutron wall loading at the blanket, rather than plasma physics, becomes the critical design restriction.

CONTENTS

LIST OF FIGURES

LIST OF TABLES

I. INTRODUCTION

The principal obstacle to the development of magnetic fusion energy as a domestic source of electric power in the United States is the high cost of the first devices that would make enough electric power to attract commercial interest. After success in large superconducting tokamak experiments, the magnetic fusion program would be positioned technically to seek commercial participation in the first magnetic fusion demonstration plant, but the participation sought would have to begin at the level of a $15B project. It is doubtful that any meaningful commercial participation could begin at that scale; the step would be too large. It is also apparent that a device of such scale will not be funded by the U.S. government alone; even large experiments must be international projects. How then can the magnetic fusion program in the United States ever begin the necessary process of government to commercial transition?

The spherical tokamak (ST) approach appears to provide an answer. The ST approach minimizes the size of a tokamak power core by discarding all non-essential components from the inner side of the plasma: no inboard blanket or shield, no inboard poloidal coil (PF) systems, no Ohmic heating (OH) solenoid. The resulting systems lie in the family of low aspect ratio tokamaks, with aspect ratio A generally considered less than 1.5. The only customary tokamak component that remains is a single turn copper toroidal field (TF) coil centerpost. Consequently, the ST shrinks to the absolute minimum size and cost tokamak fusion system. The next (small) step down in size would be to eliminate the centerpost copper rod, resulting in the spheromak.

The advantages of the spherical tokamak approach have been discussed for many years (1,2). In recent years, interest in the ST approach has grown rapidly, spawning a

number of workshops (3) and a number of new experimental machine proposals (4,5,6). Reference (7) is a valuable review of the field. The results from the START experiment (8) at Culham have been particularly influential in stimulating recent interest. START (A = 1.3) has moved the field forward into the few hundred kiloAmpere plasma current regime, observing good confinement in several hundred electron volt plasmas. START has seen plasma elongation up to 4 and the absence of major disruptions at high safety factor. The HIT device (A = 1.69) at the University of Washington (9) has reached 200 kA plasma current without the use of an OH transformer by using helicity injection current drive. These experiments and others (7) have set the stage for the proposed mega-Ampere level machines (4,5,6).

Some studies projecting the ST approach to burning plasma devices have appeared (10,11). The physics key to the attractiveness of the ST approach is in the order unity beta values promised by the combination of high elongation and low aspect ratio. The high beta values mean high power density in a small device. Indeed, in this paper, we find that the projected beta values and power densities are sufficiently high that limits on the neutron wall loading of the blankets are the determining factor in the machine size. This situation, in which the blanket technology and not the physics of the core plasma determine the device size, has been long sought and is basically the goal of magnetic fusion *plasma physics* research. The fusion power that can be produced far exceeds the Ohmic losses in the copper TF coil. Because there is no OH transformer in the ST approach, the devices are of necessity steady-state with full non-inductive current drive. Self-driven current fractions up to 90% are expected. The remaining requirement for current drive power and the TF coil Ohmic power nevertheless remain small enough to project systems with reasonable levels of plant recirculating power. Brief and favorable looks at the unusual technology aspects of the ST approach have been made. A very large advantage is the copper TF coil which can be jointed and allows a simple path to full dissassembly and replacement of all components, including the centerpost. Estimates

of the increase in resistivity of the centerpost from neutron induced transmutation indicate the possibility of a multi-year lifetime before replacement. The absence of an inboard blanket is a negligible penalty in tritium breeding or power production since the centerpost is so small it intercepts less than 5% of the fusion neutrons. The single turn nature of the centerpost requires unusual power supplies (few volts, MA currents) which appear possible. The high power density is not only a challenge to the blanket designs; it is a challenge to the divertor. Two positive aspects for the divertor have been identified. The low aspect ratio equilibria form a natural divertor with large flux expansion to lower the peak heat flux. It has also been suggested that the scrape-off layer in the low aspect ratio regime would be unusually broad (10).

In this paper, we have examined only the energetics of the ST approach. We have sought to clearly find and elucidate those physics assumptions that are needed to allow net power from a device with a copper TF coil. We have stayed with a simple, algebraic approach for as long as was conveniently possible, rather than resorting to large scoping codes, in order to more clearly display to the reader (and ourselves) the way in which the unique physics of the low aspect ratio tokamak makes possible small, high gain, copper magnet devices. We will defer to a future paper contributions to the assessment of the important technology issues raised above.

In this paper, we find that, within this ST concept, it appears (Fig. 1) possible to design a pilot plant that would only be the size of the present DIII–D tokamak and yet still produce some net electric power. At double the size of the pilot plant we have identified full 1–2 GW net electric power plants with acceptable economics. The ST approach thus has the two key features of an executable commercialization strategy: a low cost pilot plant that can attract commercial cost sharing at an affordable level and with minimal financial risk, and a strong economy of scale leading to power plants that are still small on an absolute scale.

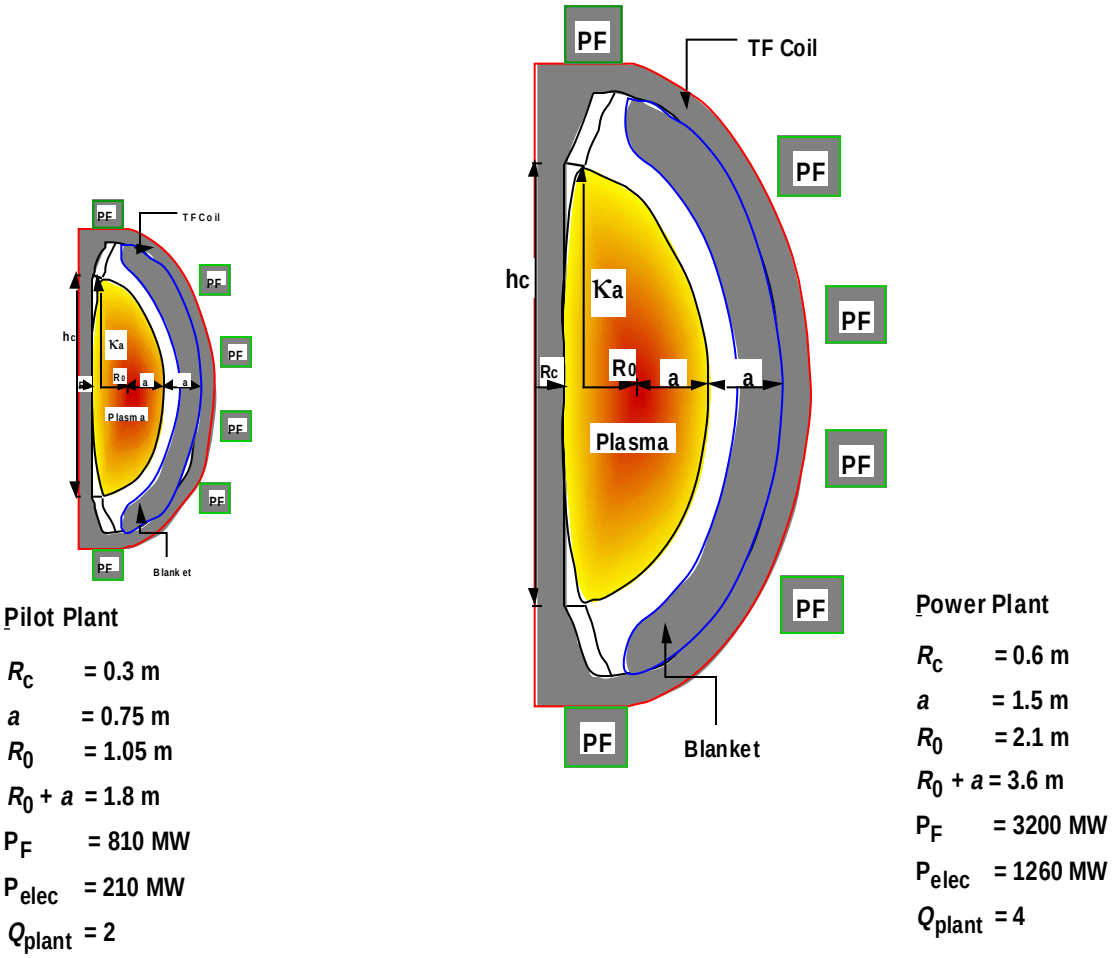

Fig. 1. An ST power plant is about twice the linear dimension of an ST pilot plant. Both cases for A = 1.4, neutron wall load at the blanket 8 MW/m^2, β_T = 62%, β_p = 1.07, f_{bs} = 0.9, κ = 2.5.

The paper is organized as follows. Section I defines the basic geometry and terms of our approach. In Section II, we develop relations for the gain of the system, defined as the ratio of fusion power to the Ohmic dissipation in the centerpost and we find that high gain systems are possible. In Section III we seek to find a limitation on the system from centerpost cooling and find that there is no practical limit to the fusion power density from centerpost cooling. In Section IV we examine the consequences of limited neutron wall loading at the blankets and find this to be the limiting factor in sizing ST devices. Finally in Section V, we implement calculations of current drive requirements and overall fusion plant energetics into a spreadsheet approach to produce integrated fusion plant

design points. We provide a brief look at prospects for burning advanced fusion fuels in large ST devices. We then provide a summary discussion and concluding remarks on the ST approach to magnetic fusion development.

II. MACHINE GEOMETRY

The geometric layout that we assume for the low aspect ratio tokamak is shown in Fig. 2. The toroidal coil (TF) centerpost is a straight cylinder of radius R_C and height h_C. In the calculations of resistive power dissipation in the centerpost (P_C), we will for convenience later take $h_C = 2a\kappa$ the height of the plasma from x-point to x-point. Later, divertor considerations will imply the centerpost might need to be 20% longer, which would increase P_C by 20%. However, as shown in the figure, the centerpost might be tapered on the ends, lowering the resistivity. These design details are left to future work.

No other space allowance is taken on the inboard side. Of course, the simplicity of the low aspect ratio approach appears primarily on the inboard side. There is no OH coil system. There are no PF coils. There is no inboard blanket or shield. The plasma is assumed to lean directly on the centerpost, which can serve as an excellent heat sink for an inboard limiter. Some space of order 0.1 m would be needed for the inboard tiles, vacuum seal surface, etc., but such details are omitted here for simplicity in the calculations.

We choose in this paper to discuss the machine performance in terms of the independent variables R_C, aspect ratio A, and elongation κ, since the centerpost power consumption is the main issue and we are interested in optimization of performance versus A The plasma major radius R_0 and minor radius a are then derived quantities.

$$R_0 = \frac{A R_C}{(A - 1)} \quad , \qquad a = \frac{R_C}{(A - 1)} \quad . \tag{1}$$

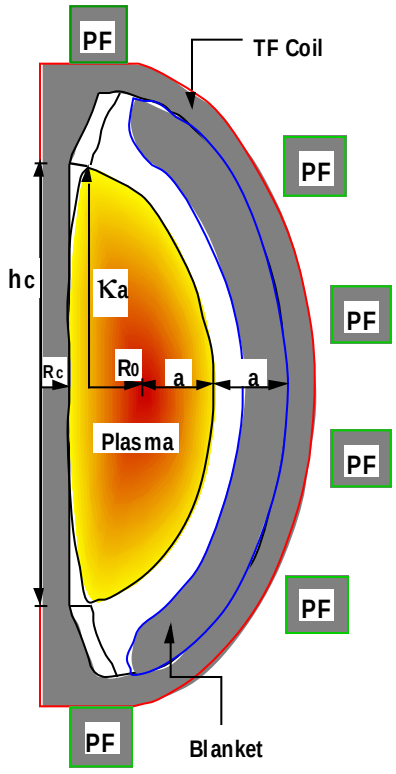

Fig. 2. Geometric layout for the low aspect ratio tokamak.

There is considerable freedom in the design of the outboard components. The removable centerpost of course necessitates TF coil joints top and bottom, making the machine easy to completely disassemble and maintain. The outer TF turns can be removed a great distance if desired for access. Their cross-section would have to increase, but their number could decrease since ripple will be very low. The PF coils can be either inside or outside the TF coil, since the TF coil is jointed. The blanket is easily serviced by TF coil disassembly or through the large gaps in the outer TF return legs. If the neutron flux on the blanket is too large, the blanket and the TF return legs can be removed to a larger radius. No detailed consideration of the design of the outboard components is given in this paper; the critical issues are all in the centerpost.

III. POWER GAIN

III.A. Fusion Power

The key issue for the low aspect ratio tokamak approach to a fusion power plant is whether a large excess of fusion power P_F can be produced relative to the resistive dissipation power in the copper toroidal field coils. The resistive power in the TF centerpost P_c is most critical since there is design freedom in the outer TF legs to make their cross-section large enough to lower the resistive power in the return legs to any desired value. In this section we will calculate a "centerpost gain" $\left(P_F/P_c\right)$ and look at optimizations.

We anticipate we need to find systems with $P_F/P_c \geq 20$ for net power breakeven. Roughly speaking we assume that the total resistive dissipation in all coils can be held to $2P_c$, that the current drive power requires another $2P_c$, and that all other plant auxiliaries require another $2P_c$. Also assuming a conversion efficiency of 1/3 for fusion power to electrical power, we obtain for the power balance in the plant $1/3\ P_F = 2P_c + 2P_c + 2P_c$ or $P_F/P_c \geq 18$.

The D-T fusion reactivity is (12)

$$\left(\overline{\sigma v}\right) = 3.68\times10^{-12}\ f(T)\ \mathrm{cm^3 s^{-1}} \quad , \tag{2}$$

$$f(T) = T^{-2/3} e^{-19.94\,\mathrm{T}^{-1/3}} \quad (\mathrm{T\ in\ keV}) \quad , \tag{3}$$

The alpha power is

$$P_\alpha = 5.6\times10^{-13} n_D n_T \left(\overline{\sigma v}\right)\ \mathrm{W/cm^3} \quad , \tag{4}$$

Then

$$\frac{dP_\alpha}{dV} = 2.06\times10^{-24}\, n_D n_T\, f(T)\ \ \mathrm{W/cm^3}\quad , \tag{5}$$

We choose the optimum D-T mix, $n_D = n_T = 1/2\, n_e$ and use n_e in units of $10^{20}/\mathrm{m}^3$

$$\frac{dP_\alpha}{dV} = 5150\, n_D^2\, f(T)\ \ \mathrm{MW/m^3}\quad , \tag{6}$$

$$P_\alpha = 5150 \int_o^a 4\pi^2 R\kappa\, n_{20}^2\, f(T) r\, dr\quad . \tag{7}$$

Using $x = r/a$ and $V =$ plasma volume,

$$P_\alpha = 5150\,(2V) \int_o^1 n_{20}^2\ f(T)\, x\, dx\quad . \tag{8}$$

We extract from the integral the central ion pressure $n_{020}\, T_0$,

$$P_\alpha = 5150\,(2V)\, n_{020}^2 T_0^2 \int_o^1 \left(\frac{n_{20}}{n_{020}}\right)^2 \frac{f(T)}{T_0^2}\, x\, dx\quad . \tag{9}$$

We take parabolic profiles

$$\left.\begin{aligned} n(x) &= n_0\left(1-x^2\right)^{S_n} \\ T(x) &= T_0\left(1-x^2\right)^{S_T} \end{aligned}\right\}\quad . \tag{10}$$

The integral is tabulated in Table I.

We choose to use in this paper profiles typical of hot ion H-mode, flat density profiles $S_n = 0$ and fairly peaked temperature profiles $S_T = 2$. The integral is not very sensitive to temperature. Over the range 10 to 30 keV, we take a typical value of 2×10^{-8}.

$$P_\alpha = 2.06\times10^{-4}\, V n_{020}^2\, T_0^2\quad . \tag{11}$$

For D-T reactions the total fusion power is $P_F = 5 P_\alpha$.

$$P_F = 1.03\times10^{-3}\, V n_{020}^2\, T_0^2\quad .$$

Table I
S_n/S_T

T	1/1	0/1	0/2	1/2	2/1	2/2
5	9.2×10^{-9}	1.31×10^{-8}	7.30×10^{-9}	5.92×10^{-9}	7.04×10^{-9}	4.96×10^{-9}
10	1.84×10^{-8}	2.78×10^{-8}	1.59×10^{-8}	1.24×10^{-8}	1.36×10^{-8}	1.01×10^{-8}
15	2.16×10^{-8}	3.41×10^{-8}	1.98×10^{-8}	1.43×10^{-8}	1.57×10^{-8}	1.19×10^{-8}
20	2.21×10^{-8}	3.58×10^{-8}	2.11×10^{-8}	1.56×10^{-8}	1.59×10^{-8}	1.22×10^{-8}
25	2.14×10^{-8}	3.56×10^{-8}	2.11×10^{-8}	1.53×10^{-8}	1.52×10^{-8}	1.19×10^{-8}
30	2.03×10^{-8}	3.43×10^{-8}	2.06×10^{-8}	1.47×10^{-8}	1.43×10^{-8}	1.13×10^{-8}

Now we wish to express P_{F} in terms of the volume average plasma β. We will use the toroidal β_{T} and the vacuum toroidal field B_{T} at the geometric center of the plasma in order to keep contact with the β-limit scaling for higher aspect ratio tokamaks (13)

$$\beta_{\mathrm{N}} \equiv \beta_{\mathrm{T}} \Big/ \left(I_{\mathrm{p}} / a B_{\mathrm{T}} \right) \quad (\%,\mathrm{MA,m,T}) \quad , \tag{12}$$

$$\beta_{\mathrm{T}} = \frac{\int n(T_{\mathrm{e}} + T_{\mathrm{i}})\, dV}{V B_{\mathrm{T}}^2 / 2\mu_0} \quad . \tag{13}$$

We take $T_{\mathrm{e}} = T_{\mathrm{i}}$ and the profiles from Eq. (10) and obtain

$$\beta_{\mathrm{T}} = \frac{4\mu_0 \, nT}{B_{\mathrm{T}}^2} \frac{1}{1 + S_{\mathrm{n}} + S_{\mathrm{T}}} \quad . \tag{14}$$

Using our profiles of choice $S_n = 0$ and $S_T = 2$ and expressing T in keV and n in $10^{20}/\mathrm{m}^3$,

$$\beta_{\mathrm{T}} = \frac{0.027 \, n_{020} \, T_0}{B_{\mathrm{T}}^2} \quad . \tag{15}$$

Using Eq. (15) in Eq. (11) and $P_F = 5P_\alpha$, we obtain

$$P_F = 1.4\left(\beta_T B_T^2\right)^2 V(\mathrm{MW,T,m^3}) \quad . \tag{16}$$

III.B. Centerpost Power

Besides the radius R_c and height h_c of the centerpost, the centerpost current I_c and current density J_c define the problem. The resistance of the centerpost is

$$R_c = \frac{\eta_c h_c}{\lambda \pi R_c^2} \quad , \tag{17}$$

where λ is the fraction of the centerpost area that is copper. The power P_c is

$$P_c = \frac{\eta_c h_c I_c}{\lambda \pi R_c^2} = \frac{\eta_c h_c J_c^2 \pi R_c^2}{\lambda} \quad . \tag{18}$$

The resistivity of copper is

$$\eta_c = \eta_{20}\left[1 + 0.41(\%/^{\circ}\mathrm{C})(T_c - 20^{\circ}\mathrm{C})\right] \quad . \tag{19}$$

The increase of resistivity with temperature is neglected herein. We use $\eta_c = \eta_{20} = 1.72 \times 10^{-2}\ \mu\Omega\mathrm{m}$, somewhat unusual units which allow us to conveniently express J_c in MA/m^2.

III.C. Centerpost Gain

The centerpost gain P_F/P_c

$$\frac{P_F}{P_c} = \frac{1.4\lambda V(\beta_T B_T^2)^2}{\eta_c h_c I_c^2 / \pi R_c^2} \ , \tag{20}$$

We use

$$B_T = \frac{\mu_0 I_c}{2\pi R_0} = \frac{0.2\, I_c\,(\mathrm{MA})}{R_0} = \frac{0.2\, J_c\, \pi R_c^2}{R_0} \quad , \tag{21}$$

and $V = 2\pi R_0 a^2 \kappa$, and $h_c = 2a\kappa$.

$$\frac{P_F}{P_c} = \frac{(1.4)(0.2)^4\, \pi^5 \lambda}{\eta_c}\, J_c^2\, \beta_T^2\, \frac{a R_c^6}{R_0^3} \ , \tag{22}$$

$$= \frac{(1.4)(0.2)^4\, \pi^5 \lambda}{\eta_c}\, J_c^2\, \beta_T^2\, \frac{R_c^4\,(A-1)^2}{A^3} \ , \tag{23}$$

III.D. β-Limit Versus *A*

Since the fusion power rises like β_T^2 it is necessary to construct a relation for the β-limit as a function of aspect ratio. From the definition the quantities involved (using poloidal circumference = $2\pi a\,(1 + \kappa^2/2)^{1/2}$, one can obtain

$$\beta_T \beta_p = 25 \left(\frac{1+\kappa^2}{2}\right)\left(\frac{\beta_N}{100}\right)^2 \quad . \tag{24}$$

Equation (24) squarely puts one of the major conflicts in present day advanced tokamak design, at any aspect ratio. One wants high β_T for fusion power. One wants high β_p for high bootstrap fraction. But β_T and β_p trade-off against each other, given conventional β-limit scaling $\beta_N = \text{constant}$. The way to increase β_T and β_p *simultaneously* is to increase κ and β_N. We have chosen $\kappa = 2.5$. We have chosen to anticipate a *specific advantage* of low aspect ratio in plasma stability by taking in this paper $\beta_N = 12/A$. Such an advantage for low A is anticipated on the basis of ballooning stability because of the increased length that a field line spends in the inboard good curvature region because β_T is so unusually high there at low aspect ratio. Recent full stability analyses (14) for $n = \infty$ ballooning and low-n kinks are supporting this

anticipation. In Fig. 3, we show the function $\beta_N = 12/A$ versus A. This function passes through the center of the range of data from DIII–D (15); $\beta_N = 6$, more optimistic than our assumed function, has been achieved transiently and is expected to be stable in steady-state in the operating mode called second stable core VH–mode (SSC-VH (16) [more recently referred to as negative central shear mode (17)]. Data on beta limits does not exist at low A. But the General Atomics group (5) have obtained equilibria stable to ideal modes at $\beta_N = 8$ to 10 at $A = 1.4$ [14], giving the range shown in the figure. We believe that such stability calculations establish a basis for $\beta_N = 12/A$. Hence

$$\beta_T \beta_p = 25 \left(\frac{1+\kappa^2}{2} \right) \left(\frac{12}{100\,A} \right)^2 = \frac{0.36\left[(1+\kappa^2)/2\right]}{A^2} \quad . \tag{25}$$

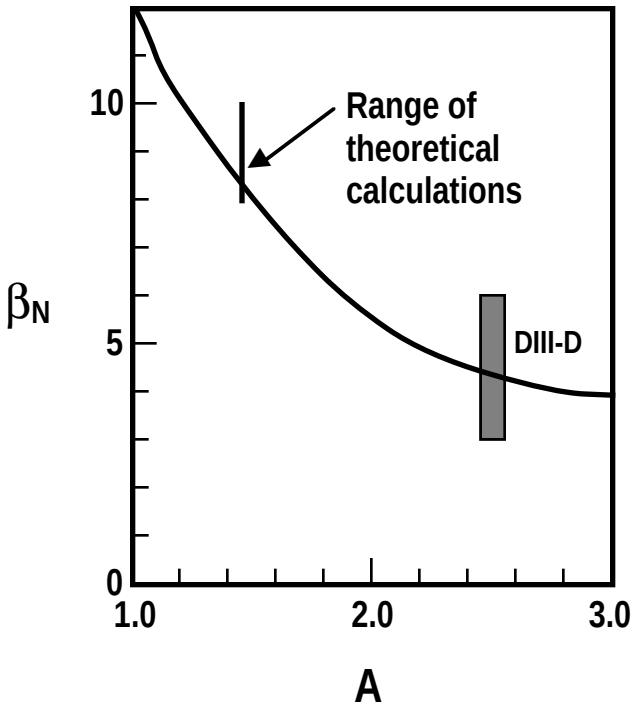

Fig. 3. Assumed relation of β_N = 12/A. Achieved values in DIII–D experiments are shown at A = 2.5. A range of theoretical calculations from Ref. (14) are shown at A = 1.4.

III.E. Optimization and Implications

We use Eq. (25) to eliminate β_T in Eq. (23).

$$\frac{P_F}{P_c} = \frac{(1.4)(0.2)^4 \pi^5 \lambda}{\eta_c} \left(\frac{0.36\left[(1+\kappa^2)/2\right]}{\beta_p} \right)^2 J_c^2 R_c^4 \frac{(A-1)^2}{A^7} \quad . \tag{26}$$

This last relation, which displays the aspect ratio dependence in the problem explicitly, implies an optimum aspect ratio given by

$$\frac{d}{dA}\left[\frac{(A-1)^2}{A^7}\right] = 0 \Rightarrow A = 1.4 \quad .$$

Taking $A = 1.4$, $\beta_p = 1$, and condensing Eq. (26),

$$\frac{P_F}{P_c} = 1.9 \lambda J_c^2 R_c^4 \quad . \tag{27}$$

A small table (Table II) of machines (with $\lambda = 1$) meeting our anticipated requirement $P_F/P_c = 20$ quickly results. Evidently we are able to find in the low aspect ratio approach small machines with substantial fusion power gain and fusion power output. The current density 20 MA/m^2 is just on the high end of conventional multi-turn hollow copper wound magnet construction. The relation Eq. (26) shows a strong increase of P_F/P_c with J_c ($\propto J_c^2$). As we will see in the section on centerpost cooling, high current densities are indeed possible.

The relation [Eq. (26)] shows a very strong economy of scale in the low aspect ratio approach since $P_F/P_c \propto R_c^4$. In this paper we present an idealized view to scope out possibilities. We do not discuss shortfalls from the ideal case, for example operating at a fraction of the β-limit, impure plasmas diluting the fuel, higher centerpost resistance, etc.

It is important to realize that such shortfalls which lower P_F/P_c can easily be made up by making the machine only slightly larger. For example, if we operate at $1/\sqrt{2}$ of the β-limit, then P_F and P_F/P_c are down a factor of two. To recover that factor of two, we only need to make the machine larger by $2^{1/4} = 1.19$, only a 19% increase in size.

Table II
Low Aspect Ratio Devices

J_c (MA/m^2)	R_c (m)	a (m)	h_c (m)	P_c (MW)	P_F (MW)
20	0.40	1.0	6.0	21	420
50	0.25	0.64	3.8	32	640
100	0.18	0.45	2.7	47	940

IV. CENTERPOST COOLING

Since $P_F/P_c \propto J_c^2$, we need to ask what limits J_c? Centerpost cooling is an obvious candidate but turns out to not be restrictive. The basic reason is that the centerpost is a short, once-through, water path.

We consider water cooling and follow the development of Montgomery (18). The temperature rise from along the length h_c of the centerpost is

$$\Delta T_{||} = \frac{(\pi R_c^2) J_c^2}{\lambda (4.186 Q)} \int_0^{h_c} \eta[T(\ell)] d\ell \quad \text{(cgs)} \quad , \tag{28}$$

where Q = volume flow rate of water,

λ = fraction of the centerpost that is copper.

This equation can be solved iteratively to correct for the temperature dependent resistivity, but we neglect such corrections in this paper.

The flow rate of the water (Q) is $\pi R_c^2 (1-\lambda) V_w$ where V_w is the linear flow velocity of the water.

$$J_c^2 = \frac{\Delta T_{||} (4.186) V_w \lambda (1-\lambda)}{\eta_c h_c} \quad . \tag{29}$$

For a given maximum ΔT and linear flow velocity of the water owing to erosion, the current density in the centerpost is maximized for λ = 1/2, a centerpost that is half water and half copper. Later it will turn out that neutron wall loading prevents the use of the maximum J_c, *i.e.*, centerpost cooling is not the limiting factor. Then the system optimization direction is to increase λ to bring down P_c at the expense of higher ΔT.

The centerpost must have multiple, closely spaced cooling passages. The temperature rise at a distance s transverse into the copper is

$$\Delta T_{\perp} = \frac{P_{\Omega}\, s^2}{2\kappa} \quad ; \qquad \kappa = 3.86 \text{ W / cm/}^{\circ}\text{C} \quad . \tag{30}$$

Using values large for our case (see Table II), $J_c = 10^4$ A/cm^2, $\Delta T_{\perp} = 22.3\,(^{\circ}\text{C/cm}^2)\,s^2$ so that to keep $\Delta T_{\perp}$ under 22.3°C, coolant passages spaced every 1 cm are required.

The pumping power required is not large. The frictional pressure drop in a tube of diameter d is

$$\Delta P\,(\text{dynes/cm}^2) = 0.49\, f\, \frac{h_c}{d}\, V_w^2 \quad , \tag{31}$$

where we take the friction factor $f = 0.04$, appropriate for $V_w \sim 300$ cm/s and fairly smooth tubes ($\Delta d/d \sim 0.016$). The pumping power per tube is

$$P\,(\text{W}) = 0.49 \times 10^{-7}\, f\, \frac{h_c}{d}\, V_w^2 \left(\frac{\pi}{4}\, d^2\, V_w\right) \quad , \tag{32}$$

using d = 1 cm, h_c = 1000 cm, V_w = 1000 cm/s, P = 1.5 kW. For the centerpost radii listed in Table II, 1000 tubes would be required, giving a total pumping power of 1.5 MW which is negligible in the level of energy balance we are discussing.

Low aspect ratio devices operated at the cooling limit of the centerpost become unreasonably small. The relation Eq. (29) expressed in the conventional units used in Section II and using $\Delta T_{||} = 100^{\circ}$C, $V_w \sim 100$ m/s, and λ = 1/2 is

$$J_c^2\,(\text{MA/m}^2) = 6.2 \times 10^4 / h_c \quad , \tag{33}$$

$$= \frac{6.2 \times 10^4}{(2\kappa)\, R_c/(A-1)} \quad .$$

Putting this relation for J_c^2 into Eq. (26)

$$\frac{P_F}{P_c} = \frac{1.4(0.2)^4\ \pi^5\lambda}{\eta_c}\left(\frac{0.36[(1+\kappa^2)/2]}{\beta_p}\right)^2 3.1\times10^4\ \frac{R_c^3}{\kappa}\frac{(A-1)^3}{A^7} \quad . \tag{34}$$

The centerpost gain now is optimized for A = 1.75. With κ = 3 and A = 1.75 and λ = 1/2

$$\frac{P_F}{P_c} = 5560\,R_c^3 \quad . \tag{35}$$

Some of the machines that result are shown in Table III. The optimization is to very small machines with enormous power outputs. Such an optimization is produced from Eq. (33) which will boost the J^2 dependence of P_F / P_c by shrinking h_c and the whole device size.

Table III
Low Aspect Ratio Devices

R_c (m)	a (m)	h_c (m)	J_c (MA/m^2)	P_F/P_C	P_F (MW)	P_c (MW)
0.1	0.133	0.8	278	5.6	370	66
0.2	0.27	1.62	197	44	11,968	272
0.3	0.40	2.4	161	150	90,600	604

For curiosity we work back through the various formulae of Section II to elaborate the R_c = 0.2 m case above (Table IV). This optimization path leads to high toroidal field (10.5 T) devices because the centerpost cooling limit supports such high J_c. Since β_T is still high (60%), extremely high power densities result. Assuming T = 40 keV, the

plasma density is enormous ($61\times10^{20}\,\mathrm{m}^{-3}$) but surprisingly still within the Greenwald density limit $n_{GR} = 63\times10^{20}\,\mathrm{m}^{-3}$.

Table IV
Parameters of $R_c = 2$ m Case

R_0	0.47 m	I_p/aB_T	5.1
a	0.27 m	I_p	14.4 MA
I_c	24.7 MA	q	>6
V_c	11 V	$n_{20}\,T_{keV}$	2.45×10^3
β_N	6.9	T_{keV}	40
β_T	0.60	n_{20}	61
B_T	10.5 T	n_{GR}	63

Even higher performance could be obtained. Since there are no insulators in the centerpost, instead of a ΔT limit of $100^\circ\mathrm{C}$, $\Delta T_{||} = 400^\circ\mathrm{C}$ might be considered. Also, although $V_w = 10\,\mathrm{m/s}$ is a high flow rate, higher V_w could be run. But the machines in Table IV are already unrealistically small; the neutron wall loading would be far beyond what blankets could handle. Centerpost cooling is simply not a limitation. But this exercise in looking at the ultimate performance of low aspect ratio tokamaks pushed to the cooling limit of the centerpost has clearly revealed the immense capability in the low aspect ratio approach for economic, high power density devices. Indeed, the neutron wall loading constraint will be shown to severely bound the use of this capability.

V. NEUTRON WALL LOADING LIMITS

Since we have found that the low aspect ratio approach can deliver extremely high power densities, it is no surprise that a neutron wall loading constraint will be the limiting factor in performance. Blanket design studies have already shown 8 MW/m^2 to be at the high end of possibility.

We take advantage of the roughly spherical shape of the ST device and assume the neutrons are emitted uniformly onto a sphere of radius $R_0 + 2a$, *i.e.*, the blanket is spaced one minor radius from the edge of the plasma. The area of the wall is

$$A_{\text{wall}} = 4\pi(R_0 + 2a)^2 = 4\pi R_{\text{c}}^2 \frac{(A+2)^2}{(A-1)^2} \quad . \tag{36}$$

Then the centerpost gain for a fixed neutron wall load ($0.8P_{\text{F}}/A_{\text{wall}}$) is

$$\frac{P_{\text{F}}}{P_{\text{c}}} = \frac{A_{\text{wall}}}{0.8P_{\text{c}}}\left(\frac{0.8P_{\text{F}}}{A_{\text{wall}}}\right)$$

$$= \left(\frac{P_{\text{F}}}{A_{\text{wall}}}\right)\frac{2\lambda}{\kappa J_{\text{c}}^2 \eta_{\text{c}} R_{\text{c}}}\frac{(A+2)^2}{(A-1)^2} \quad . \tag{37}$$

The optimization with respect to A maximizes $P_{\text{F}}/P_{\text{c}}$ at $A = 1$ (the spheromak limit!) and minimizes $P_{\text{F}}/P_{\text{c}}$ at $A = 4$. We conclude we should keep A low.

We compute the actual wall loading for operation at the β-limit.

$$\frac{0.8P_{\text{F}}}{A_{\text{wall}}} = \frac{(0.8)1.4(0.2)^4\pi^6}{4\pi}\left(\frac{0.36[(1+\kappa^2)/2]}{\beta_{\text{p}}}\right)^2 J_{\text{c}}^4 \kappa R_{\text{c}}^5 \frac{(A-1)^3}{A^7(A+2)^2} \quad . \tag{38}$$

The choice $A = 1.61$ maximizes the wall loading at the β-limit. Hence we might most easily reach the wall loading constraint at $A = 1.61$. With this consideration and the considerations of Eq. (37), we conclude $A = 1.4$ is a prudent choice. Equation (38) also shows that the family of machines with constant wall loading at some limit is defined by $J_c^4 R_c^5 = \text{constant}$. With this constraint, the centerpost gain P_F/P_c from Eq. (26) will have the size scaling $R_c^{3/2}$, a much weaker economy of scale than the robust R_c^4 considering only operation at the β-limit with a fixed J_c.

We can quickly evaluate a set of machines at the neutron wall loading limit of 8 MW/m^2. Using $\beta_p = 1,\ \kappa = 1,\ \lambda = 0.8, A = 1.4$ in Eq. (38)

$$J_c^4 R_c^5 = 1.2 \times 10^4 \quad . \tag{39}$$

Using this constraint Eqs. (39) and (27) we get a table of devices (Table V).

Despite the severity of the wall loading constraint, Table V shows an interesting family of machines, all of small size, but with high gain and fusion power output.

Table V
Devices at an 8 MW/m^2 Neutron Wall Load

R_c (m)	h_c (m)	J_c (MA/m^2)	P_F/P_c	P_c (MW)	P_F (MW)
0.2	3	78	19	49	936
0.3	4.5	60	34	60	2050
0.4	6	33	53	71	3740
0.5	9	25	74	95	7030

V.A. Trade-Off of κ Versus Size

In this paper we have treated the plasma elongation κ as a fixed ratio. There has been much discussion of the "natural" elongation properties of low aspect ratio systems. The "natural" elongation might be defined as that elongation which lies at the limit of passive vertical stability afforded by a uniform vertical field. In that case (7), κ rises as A decreases, reaching about 1.9 at A = 1.4 for flat current profiles. Most present tokamaks with elongated cross-sections operate with κ above the passive stability limit. Their control systems use a nearby conducting structure (the vacuum vessel in the case of DIII–D) to retard vertical drift times to the L/R time of the structure (~1–5 ms in DIII–D) and feedback from the poloidal coils to maintain vertical position stability on longer time scales. The limit to this control approach is reached when the plasma becomes ideal MHD unstable *even in the presence of the conducting structure*. This limit was evaluated in Ref 19 for customary conducting wall positions and fairly peaked, ohmic current profiles in the aspect ratio range 2.0–6.0 and found to be, $\kappa = 2.5$, almost constant but slowly rising as A falls. Some preliminary calculations we have made indicate that $\kappa = 3$ may be the feedback stability limit at A = 1.4 with peaked current profiles. The maximally stable κ should rise as the current profile is broadened. Hollow current profiles (the negative central shear regime) are required for the high values of β_N we have postulated. From these considerations, our choice $\kappa = 2.5$ is probably a conservative choice of what can be achieved with feedback control. Feedback control may be more possible in the spherical torus than in a superconducting tokamak since one does not have the feature of eddy current heating of a superconducting TF coil being produced by time changing PF system currents. We await theory calculations like those of Ref. 19 to be extended into the low aspect ratio regime. The result is likely a dependence of κ on A. Also likely is a systematic dependence of β_N on κ on A. When such relations for κ (A) and β_N [κ (A)] are available, their inclusion in the formalism of this paper would result in

a different optimum A (no doubt lower A and higher κ) than the value A = 1.4 we have found optimum.

Nevertheless, within the framework of this paper we can consider the choice of κ a free design choice (up to about 3) and ask what the trade-off of κ and device size is. The ST approach is efficient at shrinking the horizontal dimension of the device, but somewhat at the expense of raising the vertical dimension. We might expect the cost to scale roughly like the volume of the machine, or plasma, and examine the variation of the plasma volume with κ versus minor radius as we hold constant the centerpost gain P_F/P_C. The centerpost gain at the β limit is given by Eq. (26). The centerpost gain at the wall loading limit is given by Eq. (37). Equating these two expressions gives the trade-off relation for operating at the beta limit and the wall loading limit simultaneously.

$$J_c^4 R_c^5 \left(\frac{1+\kappa^2}{2}\right)^2 \kappa = \text{constant} \tag{40}$$

If we fix J_C, then the machine size must vary as

$$R_c\,(\text{size}) \propto \left[\left(\frac{1+\kappa^2}{2}\right)^2 \kappa\right]^{-1/5} \tag{41}$$

Increasing κ from 2.5 to 3.0 would allow decreasing R_C by 18%. Dropping κ to 2.0 would require increasing R_C by 21%. The plasma volume is proportional to $R_c^3\,\kappa$ which becomes

$$\text{Volume} \propto \left[\left(\frac{1+\kappa^2}{2}\right)^2 \kappa\right]^{-3/5} \kappa \quad . \tag{42}$$

From Eq. (37) the centerpost gain is proportional to $(R_C\,\kappa)^{-1}$, which becomes

$$\text{Gain} \propto \left[\left(\frac{1+\kappa^2}{2}\right)^2 \kappa\right]^{-1/5} \kappa^{-1} \quad . \tag{43}$$

From Table VI we see that as we raise κ from 2 to 3, we decrease the linear dimension of the machine by 0.42/0.60 = 0.7 and decrease the volume by 0.22/0.44 = 0.5 and only slightly (0.79/0.83 = 0.95) decrease the gain. Since increasing κ from 2 to 3 is able to effect a factor 2 reduction in plasma and machine volume, we have strong motivation to increase the elongation.

One could try to compensate for lower elongation by keeping the size R_C constant but increasing the centerpost current density. The trade-off relation is

$$J_C \propto \left[\left(\frac{1+\kappa^2}{2}\right)^2 \kappa\right]^{-1/2} \kappa^{-1} \quad . \tag{44}$$

Since the gain [from Eq. (37)] goes as $\left(J_C^2\,\kappa\right)^{-1}$ the gain is proportional to

$$\left[\left(\frac{1+\kappa^2}{2}\right)^2 \kappa\right]^{-1/2} \kappa^{-1} \quad . \tag{45}$$

When κ is decreased from 3 to 2, the gain would decrease by a factor 1.6. Increasing J_C as κ decreases is not a desirable trade-off path because it costs too much gain.

Table VI
Trade-Off Factors

κ	Size Factor	Volume Factor	Gain Factor
2.0	0.60	0.44	0.83
2.5	0.50	0.31	0.80
3.0	0.42	0.22	0.79

VI. INTEGRATED DESIGNS

Since the analysis of the previous section did find an interesting set of machines within the wall loading constraint, we press on to construct a complete plant model in a spreadsheet. We document here the relations used in the spreadsheet and display the results as a set of figures later.

VI.A. Geometry

The geometry of the machine is as described in Section I with the independent variables R_c, A, and κ (= 2.5 throughout). All other variables are derived. To be consistent with the high stability requirements for β_N, a plasma triangularity $\delta = 0.8$ is assumed but plays no role in the power balance calculations herein.

VI.B. Centerpost

The centerpost height is assumed to be $h_c = 2a\kappa$. The current density J_c is assumed and adjusted to give the specified wall loading power. The toroidal field is $B_T = 0.2\, I_c/R_0$. The mass and weight of the centerpost are calculated ($\rho_{cu} = 8.96 \times 10^3$ kg/m^3). The centerpost is assumed to be 80% copper, $\lambda = 0.8$. No correction is made for the temperature dependence of the copper resistivity. A water flow velocity V_w = 10 m/s is assumed. The temperature rise is calculated from Eq. (29) and is never large for the machines to be shown.

VI.C. TF Return Legs

The outer legs of the TF coil are taken as half-circles at a radius $R_{out} = R_0 + 2a$ and their cross-section is sized to obtain a resistive dissipation equal to a specified fraction $f_R = 0.5$ of the centerpost power. Twelve return legs are taken and the resulting cross-sections are modest (0.2 to 0.6 m on a side). The voltage drop on the return leg is added to the centerpost voltage drop to obtain a total voltage drop on the TF coil, V_{TF}, which ranges from 8 to 7 V for the range of machines to be shown. Since we envision semiconductor power supplies for the TF with an unavoidable internal voltage drop of about 1 V, we take the electrical efficiency of the TF power supply to be 0.9 $\left(1-1\mathrm{V}/\mathrm{V}_{TF}\right)$.

VI.D. Fusion Power and Wall Loading

The fusion power is computed from

$$P_F\,(\mathrm{MW}) = 1.4(2)(0.2)^4\,\pi^6 \left(\frac{0.36[(1+\kappa^2)/2]}{\beta_p}\right)^2 J_c^4\,\kappa\,R_c^7\;\frac{(A-1)}{A^7}\;, \qquad (46)$$

and the wall loading using a wall area given by Eq. (36). J_c is adjusted to obtain a specified P_F/A_{wall}. The ratio P_F/P_c is calculated. The alpha power P_α is $P_F/5$.

VI.E. Plasma Parameters

Beta poloidal is selected to give a high bootstrap current fraction (see Current Drive section below). The β_T is calculated from Eq. (25)

$$\beta_T = \frac{0.36[(1+\kappa^2)/2]}{\beta_p}\;,$$

and β_N.= 12/A. Then $I_p/aB_T = 100\beta_T/\beta_N$ and $I_p\,(\mathrm{MA}) = aB_T\left(I_p/aB_T\right)$. Two estimates of the safety factor are made.

$$q_1 = \frac{a^2 B_T}{0.2\,R_0 I_p}\left(\frac{1+\kappa^2}{2}\right)\left\{1+\frac{1}{A^2}\left[1+\frac{(\beta_p+\ell_i/2)^2}{2}\right]\right\} \quad , \tag{47}$$

$$q_2 = \frac{a^2 B_T}{0.2\,R_0 I}\left(\frac{1+\kappa^2}{2}\right)\frac{A}{A-1} \quad . \tag{48}$$

We find $q_1 \cong 2\times q_2$, and $q_1 > 5.8$ for all the machines to be discussed. The safety factor is not restrictive. The magnetic energy stored in the plasma is

$$W_m = \frac{1}{2}\,\mu_0\,R_0\,\ell_i\,I_p^2 \ , \tag{49}$$

and ranges from 20 to 600 MJ. The kinetic energy stored in the plasma is

$$W_k = 3\beta_T\,B_T^2\ \mathrm{V}/(1.6\,\pi) \quad , \tag{50}$$

and ranges from 30 to 1000 MJ. The product $n_{20}T_{\mathrm{keV}}$ is computed from Eq. (15)

$$n_{20}T_{\mathrm{keV}} = 37.5\beta_T\,B_T^2 \ .$$

We assume $T_{\mathrm{keV}} = 45$ keV and calculate the density n_{20},which ranges from 4 to $2\times10^{20}\,\mathrm{m}^{-3}$. These densities range from 0.4 to 0.8 times the Greenwald limit $n_{GR} = I_p\,(\mathrm{MA})/\pi a^2$.

VI.F. Current Drive

We specify the bootstrap fraction $f_{bs} = 0.9$ and compute $\beta_p = f_{bs}\sqrt{A}$.

We compute the power required to drive the remainder of the current $I_{CD} = I_p(1 - f_{bs})$ following Tonon (20). We compute the volume average density and temperature from the assumed profiles [Eq. (10)].

$$\bar{n} = n_{020}/(1+S_N) \;; \qquad S_N = 0 \;,$$

$$\bar{T} = T_0/(1+S_T) \;; \qquad S_T = 2 \;. \tag{51}$$

Then

$$P_{CD} = \frac{\bar{n} R_0 I_{CD}}{\gamma} \;, \tag{52}$$

where γ is the usual current drive figure of merit. We use

$$\text{NBCD:} \quad \gamma_{NB} = 0.25\bar{T} \;, \tag{53}$$

$$\text{FWCD:} \quad \gamma_{FW} = \left[0.063\,\bar{T}/(2+Z_{eff})\right]\left((1+\beta_T/2\right) \;, \tag{54}$$

$$\text{LHCD:} \quad \gamma_{LH} = 0.037 B_T\,\bar{T}/\left(5+Z_{eff}\right)\bar{n}^{1/3} \;, \tag{55}$$

$$\text{ECCD:} \quad \gamma_{EC} = 0.09\bar{T}/\left(5+Z_{eff}\right) \;. \tag{56}$$

We used $Z_{eff} = 1$. We do not go into the physics constraints on these techniques herein. We do note LHCD has an accessibility problem and ECCD has challenges at these combinations of n and B_T.

VI.G. Helicity Injection Current Drive

Because these low aspect ratio machines have a low B_T and high n, the rf and NB current drive schemes suffer in efficiency. Hence we looked at helicity injection current drive derived from an electrode as in the HIT experiment (19). Current profiles from

HICD tend to be flat so we compute the Ohmic dissipation in the plasma assuming a flat current profile in the presence of a temperature profile given by

$$T_e(r) = T_0\left[1-\left(1-T_b/T_0\right)(r/a)^2\right]^{S_T} \quad , \tag{57}$$

and obtain approximately for $S_T = 2$

$$P_{OH}\,(\mathrm{MW}) = \frac{0.028\pi R_0^2\, I_p^2\ (\mathrm{MA})}{\pi a^2 \kappa}\,\frac{1}{T_0^{3/2}}\left(\frac{T_0}{T_b}\right)^2 \quad . \tag{58}$$

We have taken $Z_{eff} = 1$. The values P_{HICD} that result range from 30 to 60 MW. It is interesting to back out the electrode current and voltage requirements. The electrode current is

$$I_{el} = \left(\frac{\lambda_{el}}{\lambda}\right)\frac{I_p}{\psi_T}\,\psi_{el} \quad , \tag{59}$$

where (λ_{el}/λ) is a current efficiency factor taken to be 2, ψ_{el} is the current carrying poloidal flux linking the electrode, and ψ_T is the toroidal flux $= \pi a^2\,\kappa\,B_T$.

$$\psi_{el} = 2\pi R_0\,(\Delta R)_{SOL}\,B_p \quad , \tag{60}$$

$$B_p = \frac{0.2\,I_p}{a\sqrt{\dfrac{1+\kappa^2}{2}}} \quad . \tag{61}$$

We take ΔR_{SOL} to be 0.01 m. Then $V_{el} = P_{HICD}/I_{el}$. For the machines considered herein, I_{el} = 0.3 to 0.25 MA and V_{el} = 90 to 250 V.

VI.H. Divertor Considerations

Because these machines have high power density, they also pose a severe divertor challenge. The power crossing the separatix is

$$P_{\mathrm{SOL}} = P_{\alpha} + P_{\mathrm{CD}} - P_{\mathrm{BR}} - P_{\mathrm{RAD}} \quad , \tag{62}$$

where P_{BR} is the bremsstrahlung power

$$P_{BR} = \left(2.67 \times 10^{-3}\right) V Z_{\mathrm{eff}} n_{20}^{2} T_{\mathrm{keV}}^{1/2} \quad , \tag{63}$$

and we assume P_{RAD} = 25% of the sum of $P_{\alpha} + P_{\mathrm{CD}}$. We calculate the index of divertor power handling P/R_0 and find values ranging from 100 to 250 MW/m; P/R_0 in ITER is $\sim$40 MW/m.

We assume a divertor plasma marginally limited on the inner wall so that 50% of $P_{\alpha} + P_{\mathrm{CD}}$ goes to the centerpost giving average power fluxes to the inner wall $\cong$10 MW/m^2.

The remainder of the power, 50% of P_{SOL}, is considered to flow into only the two outer legs of a double null divertor. We assume a radiative divertor uniformly illuminating the surfaces in these divertors to an average 10 MW/m^2 and calculate the poloidal length of the divertor needed to make this true. That length is typically 15% of h_{c}.

VI.I. Confinement Requirements

The viewpoint taken to this point has been to examine operation at the β-limit. Hence we know the stored energy in the plasma. The total heating power $P_{\alpha} + P_{\mathrm{CD}}$ has also been calculated, so we can calculate the energy confinement time required to provide

a steady-state at the β-limit. Those confinement times are then compared to the ITER89–P L–mode scaling (21)

$$\tau_{89P} = 0.048\, I_p^{0.85} R_0^{1.2} a^{0.3} \bar{n}^{-0.1} B_0^{0.2} \left(m_{DT}\, \kappa / P_{HEAT}\right)^{1/2} \quad , \tag{64}$$

to define $H = \tau_E / \tau_{89P}$ and to the present ITER H–mode confinement assumption (22)

$$\tau_{ITER\,H} = 0.036\, I_p^{1.06} B_0^{0.32} P_\alpha^{-2/3} n_{020}^{0.17} m_{DT}^{0.41} R_0^{1.9} a^{-0.11} \kappa^{0.66} \quad , \tag{65}$$

to define $VH = \tau_E / \tau_{ITER\,H}$.

VI.J. Overall Plant Efficiency

We wish to translate the calculated values of heating power, TF coil power, and fusion power into an overall plant electrical efficiency $Q_{PLANT} \equiv$ gross electrical power output/electrical power to run the plant. Again we follow Tonon (20). The electrical efficiency of the current drive system is taken as $\eta_{CD} = 0.4$. The electrical efficiency of the TF power system η_{TF} was taken as $0.9\left(1 - 1/V_{TF}\right)$ as discussed earlier. All other plant systems are assumed to require 7% of the gross electric power generated. So the power recirculating in the plant is

$$P_{RECIRC} = P_{CD}/\eta_{CD} + P_{TF}/\eta_{TF} + 0.07\, P_{GROSS,E} \quad . \tag{66}$$

To compute the gross electric output, a blanket multiplier $M = 1.25$ was taken. It was also assumed that 50% of the power collected as heat $\left(P_\alpha + P_{CD,E} + P_{TF,E}\right)$ could be taken into the thermal cycle. The efficiency of the thermal cycle was taken as 46%. The gross electric power is

$$P_{GROSS,E} = \left[M\left(P_F - P_\alpha\right) + 0.5\left(P_\alpha + P_{CD,E} + P_{TF,E}\right)\right] / 0.46 \quad , \tag{67}$$

$$Q_{\mathrm{PLANT}} = P_{\mathrm{GROSS,E}}/P_{\mathrm{RECIRC}} \quad . \tag{68}$$

The net electric power is $P_{\mathrm{GROSS,E}} - P_{\mathrm{RECIRC}}$.

VI.K. Resulting Machines

The low aspect ratio path does contain a small pilot plant type device and an attractive economy of scale to power plants. All of the designs considered have in common

$A = 1.4$

$\beta_T = 62\%$

$\beta_p = 1.07$

$f_{\mathrm{bs}} = 0.90$

$\kappa = 2.5$

Neutron power at Blanket = 8 MW/m^2.

Figure 4 shows P_F/P_c and Q_{PLANT} versus machine size as gauged by R_c. At the low end, $R_c \sim 0.2$ to 0.3 m, we find devices with $P_F/P_c = 8$ to 14 and $Q_{\mathrm{PLANT}} = 1.3$ to 1.8. Such devices are minimum size and cost pilot plants. At larger $R_c = 0.6$ to 0.7 m, we find a suitable range for a power plant with $P_F/P_c = 40$ to 50 and $Q_{\mathrm{PLANT}} = 3.8$ to 4.4. In Fig. 5, we see the pilot plant makes a fusion power in the range 400 to 800 MW and a net electric power in the range 50 to 200 MW. The power plants make fusion power 3000 to 4000 MW and net electric power in the 1000 to 2000 MW range.

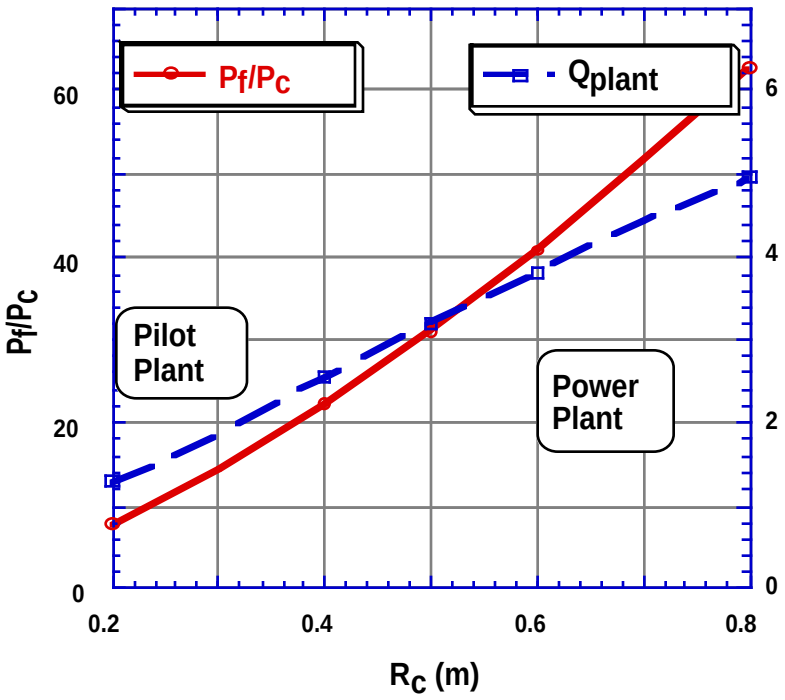

Fig. 4. The ST approach contains a small pilot plant with plant Q = 1–2 and a strong economy of scale to power plants with a plant Q = 4–5.

These are all small devices. In Fig. 6 we see the pilot plant has $R_0 = 0.7$ to 1.0 m and $a = 0.5$ to 0.8 m. The power plants have $R_0 = 2$ to 2.5 m and $a = 1.5$ to 1.8 m, compared to ITER at $R_0 = 8.2$ m and $a = 3$ m.

The wall loading constraint forces J_c to decrease as R_c increases as shown in Fig. 7. The pilot plants have $J_c = 80$ to 50 MA/m^2 and toroidal fields 2.9 to 2.7 T. The power plants have $B_0 = 2.2$ to 2.1 T and $J_c \sim 20$ MA/m^2, a technically low value that only produces about a 10°C rise in the centerpost cooling water temperature. The centerpost power ranges from 50 MW in the pilot plant to 90 MW in the power plant.

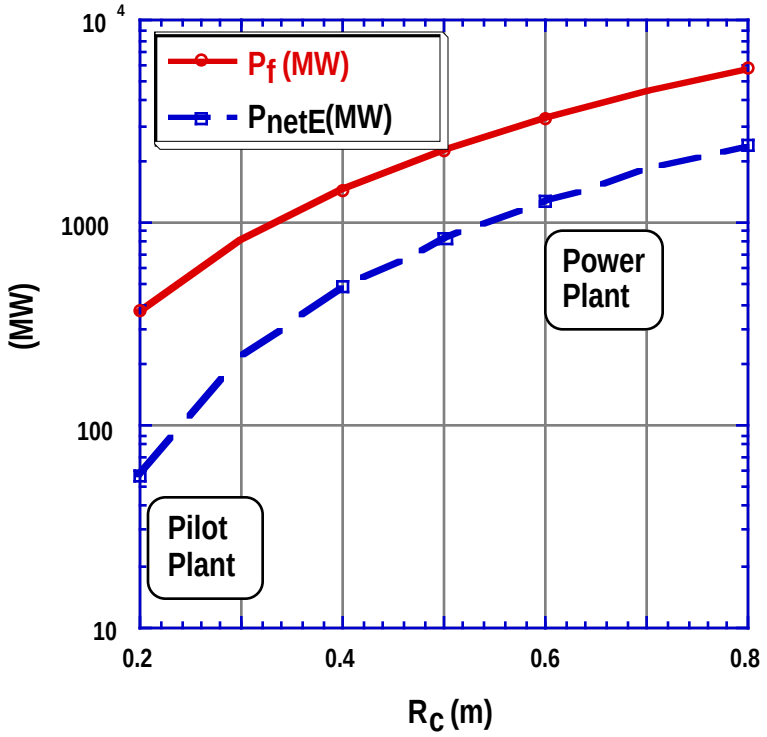

Fig. 5. Pilot plants make 50–250 MW net electric. Power plants make 1000–2000 MW net electric.

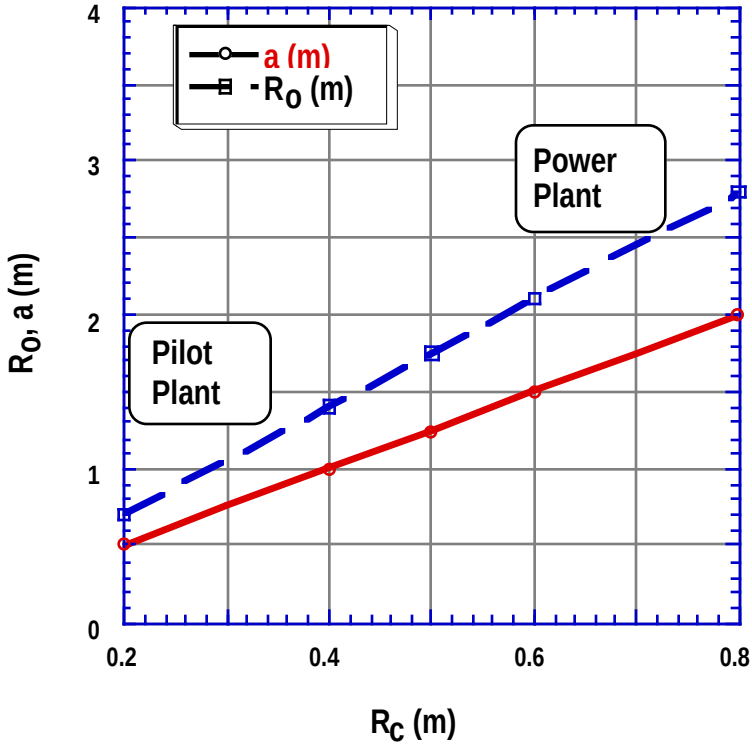

Fig. 6. Plasma size parameters: All for $\kappa = 2.5$, $A = 1.4$, centerpost height $h_c = 2a\kappa$.

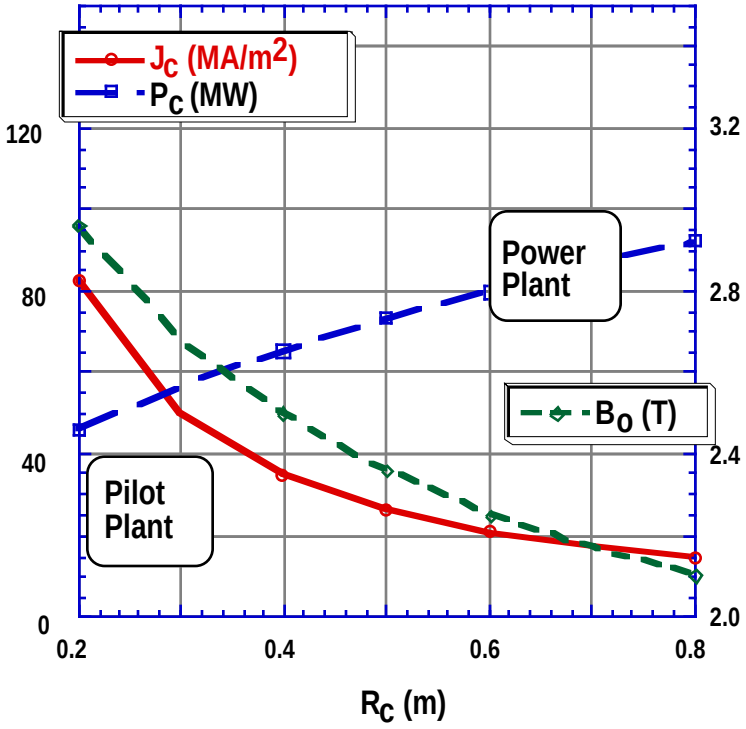

Fig. 7. Allowable neutron wall loading (8 MW/m^2) forces J_C and B_O to decrease with increasing R_C, $\beta_T = 62\%$, $\beta_p = 1.07$, $f_{bs} = 0.9$.

The plasma parameters are summarized in Fig. 8. With a 45 keV assumed central temperature, required densities range from 4×10^{20} to 2×10^{20} m^{-3}, corresponding to 0.4 to 0.8 times the Greenwald limit. The plasma current ranges from 10 to 15 MA in the pilot plant to 25 MA in the power plant. The current drive power range is from 40 to 70 MW. The absolute energy confinement times (Fig. 9) are reasonable, ranging from 0.3 to 0.7 s. When these values of τ_E are compared to the ITER L– and H–mode scalings, confusion results. The problem is that these scalings have no basis at $A = 1.4$ and the H–mode scaling predicts a τ_E about half of L–mode at $A = 1.4$, which makes no sense. In Fig. 10 we see an H factor of 3.5 in the pilot plant range is required and $H = 2.5$ in the power plant range. However, apparently $VH = 4.5\times\tau_{\text{H-MODE}}$ is required for the pilot plant and $VH = 3.3$ for the power plant! Clearly we require energy confinement data at low A to have any basis for discussing the confinement adequacy of these machines.

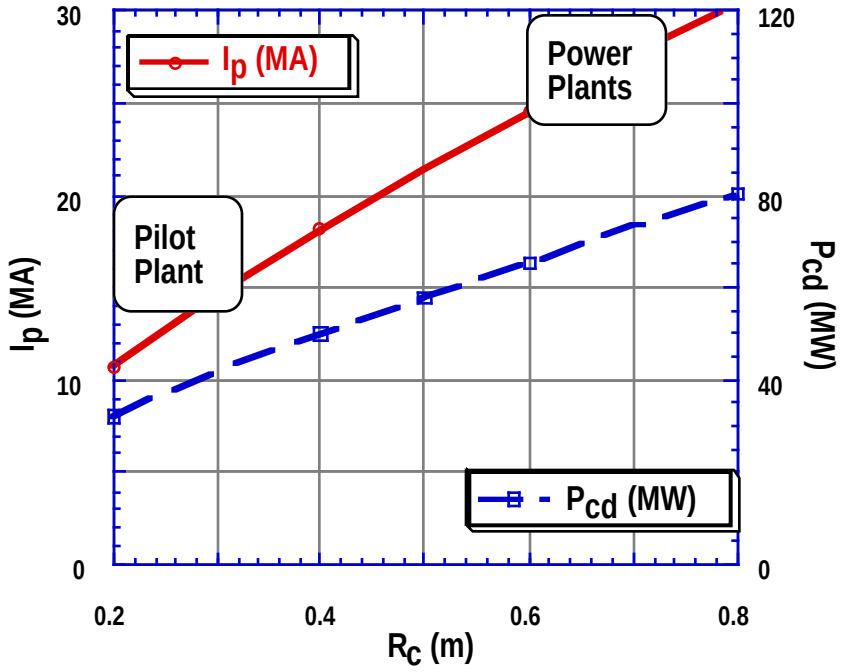

Fig. 8. Plasma current and current drive power needed to drive 10% of the current.

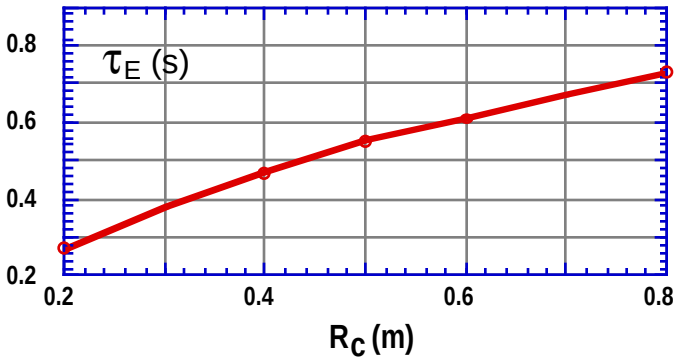

Fig. 9. Absolute energy confinement times.

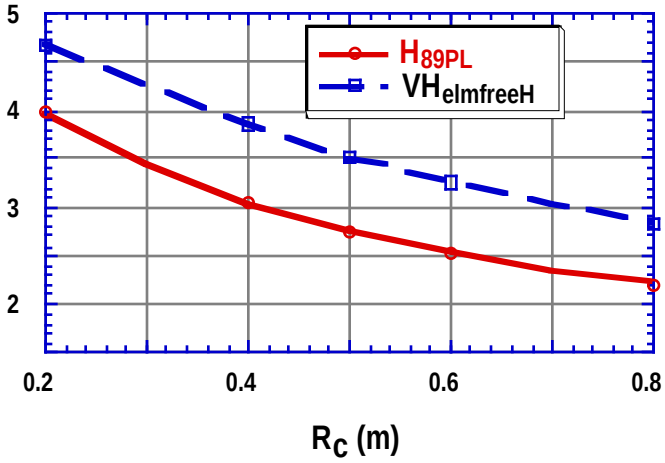

Fig. 10. Confinement enhancement factor (H) over ITER–89P L–mode scaling and (VH) over ITER H–mode scaling.

The various current drive powers are shown in Fig. 11. Neutral beams and fast waves are all competitive in a reasonably low range. For the overall current drive power, we took the average of the neutral beam and HICD results.

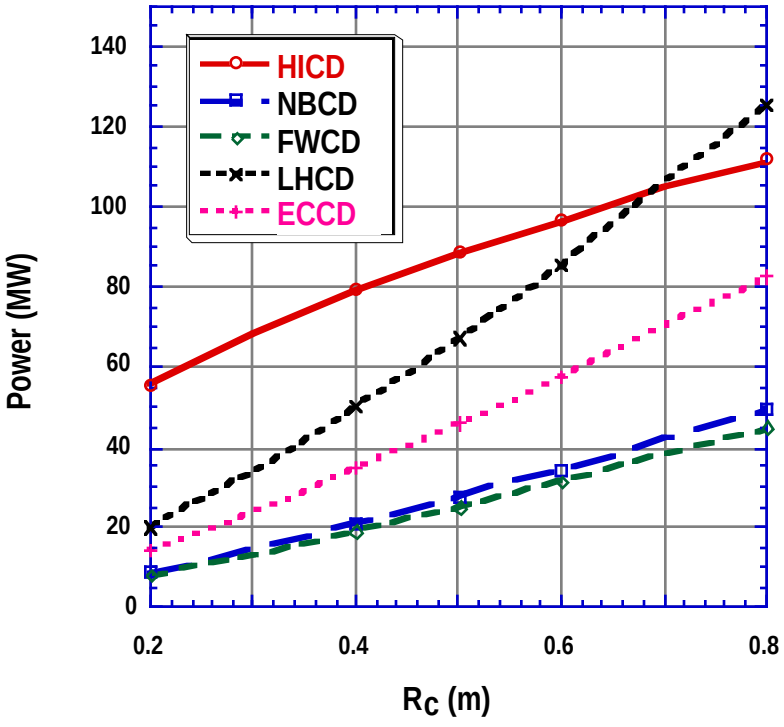

Fig. 11. Current drive power required using various techniques.

The divertor situation is summarized in Fig. 12. P/R ranges from 100 to 250; in ITER $P/R \sim 40$. The poloidal length of the divertor needed to produce 10 MW/m^2 uniform heat flux ranges from 0.5 to 1.3 m and is always about 15% of h_c (Fig. 13).

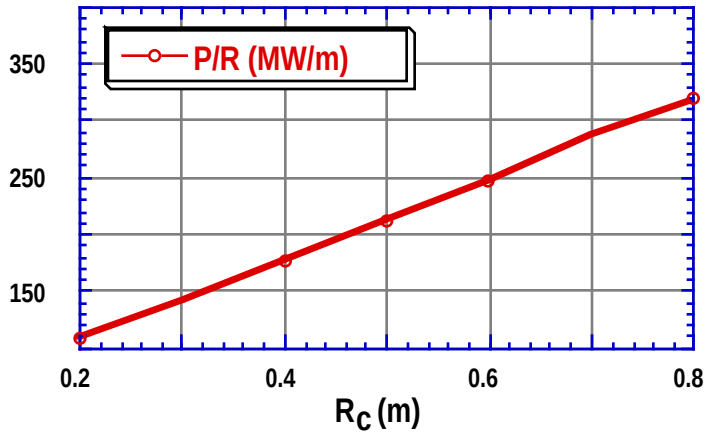

Fig. 12. P/R values range from 2–8 times ITER.

VI.L. Prospects for Advanced Fuel Burning

As was evident in the discussion in Sections III and IV, the ST approach has a very strong scaling of gain P_F/P_C with machine size ($\alpha\ R_c^4$). This strong size scaling quickly leads to absurdly high fusion power output and very high gain in devices of the ITER class burning D-T. The question naturally arises as to whether there is enough excess capacity in the ST at large size to burn advanced fuels like D-He^3 despite their lower reactivity. A D-He^3 system can produce as low as 1% of the neutrons from a D-T system, effectively removing centerpost radiation damage as a design issue.

We need to develop the formula for fusion power from D-He^3 in terms of β. The reaction ^{3}He (d, P) ^{4}He liberates 18.3 MeV in charged particles (12). The power released in charged particles is

$$\frac{dP_{CH}}{dv} = 2.9\times10^{-12}\, n_D\, n_{He3} \left(\overline{\sigma v}\right) \text{ (W/cm}^3\text{)} \quad . \tag{69}$$

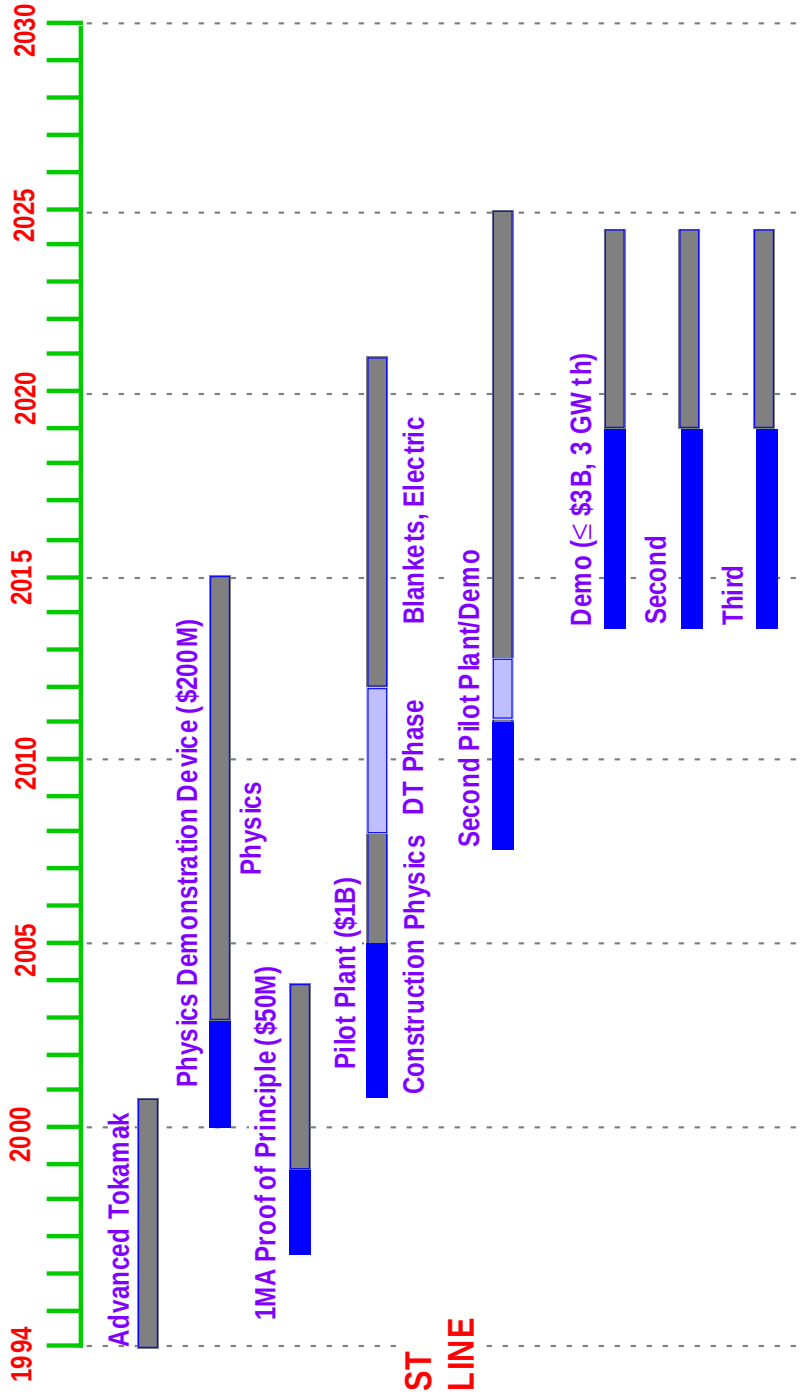

Fig. 13. Poloidal length of divertor to receive 10 MW/m^2 on both sides of both legs of a double-null, assuming 1/2 the power goes to the inner wall.

Since $n_D + 2n_{He^3} = n_e$, $n_D = n_{He^3} = \frac{1}{3} n_e$.

$$\frac{dP_{CH}}{dv} = 2.9 \times 10^{-12} \left(\frac{1}{9}\right) n_e^2 \left(\overline{\sigma v}\right) \quad . \tag{70}$$

To define the integral as in Eq. (9), we express the density in units 10^{20} m^{-3}.

$$P_{CH} = \left(3.22 \times 10^{15}\right)(2V) n_{020}^2 T_0^2 \int_0^1 \left(\frac{n_{20}}{n_{020}}\right) \frac{\overline{\sigma v}}{T^2} x \, dx \quad . \tag{71}$$

To evaluate the integral defined by Eq. (71), we use the formula for $\overline{\sigma v}$ from Ref. 23.

$$\ell n(\overline{\sigma v}) = a_0 + a_1 \ell n T + \ldots a_4 (\ell n T)^4 \quad . \tag{72}$$

T is in eV and $\overline{\sigma v}$ in m^3/s

a_0 = –376.4996

a_1 = 106.3946

a_2 = –14.27170

a_3 = 0.9198107

a_4 = –0.02336779

We have calculated a portion of Table I for the profiles used in this paper, S_n = 0, S_T = 2 and record the results in Table VII.

Table VII
$\left(\overline{\sigma v}\right)$ for D-He^3

T (keV)	$\left(\overline{\sigma v}\right)$ (m^3/s)
20	0.54×10^{-21}
40	1.45×10^{-21}
60	1.9×10^{-21}
80	2.0×10^{-21}
100	1.9×10^{-21}

We take a value of $\overline{\sigma v} = 2 \times 10^{-21}$ and remember to consider that the temperature must be taken above 60 keV. We obtain

$$P_{CH} = 1.29 \times 10^{-5}\ V n_{020}^2 T_0^2 \tag{73}$$

analogous to Eq. (11), however the numerical coefficient is 77.6 times lower than the total fusion power for D-T reactions.

We also need to correct the formula for β to reflect the deficit of ions compared to electrons.

$$n_e T_e + n_i T_i = n_e \left(T_e + \frac{2}{3} T_i \right) \tag{74}$$

Instead of Eq. (15) we have $\beta_T = 0.0225\ n_{020}\ T_0 / B_T^2$ and instead of Eq. (16) we have

$$P_F = 0.0255\ \left(\beta_T B_T^2\right)^2 V \text{ (MW, T, m}^3\text{)} \quad . \tag{76}$$

The D-He^3 fusion power output is 55 times less then the D-T output at the same β_T. In all formulas after Eq. (16), whenever the numerical factor (1.4) appears, we need to substitute 0.0255 to get the corresponding formula for D-He^3. The consideration of

neutron loading of blanket surfaces in Section V must be turned into a consideration of charged particle power on the first wall.

The basic difficulty with realizing an effective D-He^3 system is a surprising one; for systems with high gain, the absolute value of the fusion power produced is too large. To see this, we note from Eq. (26) that since the fusion power from D-He^3 is down by a factor 55 compared to D-T, to get the same gain P_F/P_C we must increase the size of the machine like $R_C \alpha (55)^{1/4}$, as we anticipated using the R_C^4 dependence of the gain to find a large but effective D-He^3 system. Unfortunately from Eqs. (16) or (46), we find that the fusion power output scales like R_C^7. Hence the ratio of the fusion power in our larger D-He^3 device to the fusion power in our smaller D-T power plant will be

$$\frac{P_{D-He^3}}{P_{D-T}} = \frac{1}{55}\left[(55)^{1/4}\right]^7 = (55)^{3/4} = 20 \quad . \tag{76}$$

Even though the D-He^3 reactivity is so much lower than D-T, we get 20 times more fusion power out at the same gain P_F/P_C!

This remarkable outcome became quickly apparent from using the modified integrated system design spreadsheet. Of course, to reduce the fusion power, one decreases J_C, but then the gain is also reduced. We have not been able to find a sensible set of parameters for a copper TF coil ST burning D-He^3. One is led to a parameter space with R_C ~ 2.7 m, R_O ~ 9.4 m, a ~ 6.7 m, B_O ~ 2.7 T, and J_C ~ 5.6 MA/m^2. In such systems, the centerpost is absolutely very large and the current density is extremely low. The possibility would seem to exist to easily replace the copper TF coil with a superconducting TF coil and within the space envelope afforded by R_C = 2.7 m easily include a cryostat and neutron shield. This step eliminates the ohmic dissipation in the TF from the power balance and allows a D-He^3 system at a fusion power output of 11 GW with a plant Q = 4. A parameter list for such a system is below:

Superconducting D-He^3 Plant

R_C	2.7 m
A	1.4
a	6.75 m
R_O	9.45 m
κ	2.5
J_C	5.6 MA/m^2
Fusion power	11 GW
Q plant	4
Net electric power	4 GW
Current drive power	390 MW
Plasma current	133 MA
B_o, field on axis	2.7 T
τ_E	5 s
H (over ITER–89P)	2
P_F/A_{wall}	3.4 MW/m^2
β_T	62%
β_p	1.07
f_{bs}, bootstrap fraction	0.9
β_N	8.6
I/aB	7.3 (MA,m,T)
T (0)	100 keV
n (0)	2×10^{20} m^{-3}

From this cursory look at burning D-He^3 in an ST device, it would appear there is some possibility in large device sizes if the copper TF coil is replaced with a superconducting TF coil. Space for a cryostat and shield is available especially considering the low neutron rates from D-He^3 burning.

VII. SUMMARY DISCUSSION OF KEY ISSUES

In this paper, we have examined the potential of spherical tokamak systems to reduce the size of magnetic fusion power systems. Meaningful size reductions in the tokamak line require elimination of inner bore components. The spherical tokamak discards the inner blanket and shield and the Ohmic coil systems. Without an inner blanket and shield, the toroidal coil cannot be superconducting; it must be a single turn copper construction. In this paper, we have concentrated on the energetics of the system, addressing the key question of whether enough fusion power density can be obtained in the spherical tokamak to make up for the Ohmic dissipation in the copper toroidal field coil. We have found a positive answer, indeed a potentially exciting line of development through small pilot plants to full power plants. In this section, we summarize the development in this paper, calling attention to important approximations made in order to define useful paths of future work. We also summarize the critical R&D elements needed to prove out the spherical tokamak approach and enable pursuit of the development path we have outlined.

We discussed a class of machines with self similar geometry, fixed aspect ratio and elongation, in which case one linear dimension characterizes the device size. We chose to present our discussion in terms of the radius of the copper centerpost, R_C, since the Ohmic dissipation in the centerpost is the primary quantity of interest. We defined the key figure of merit for the ST system as the "centerpost gain," defined as the ratio of fusion power to Ohmic dissipation in the centerpost. Our approach was to examine the ultimate performance of the ST approach by examining operation at the beta limit and the neutron wall loading limit at the blanket. We sought and found systems with that gain P_F/P_C greater than 20 in the belief that a net electric power system could then result. We

carried the analysis forward to a full plant calculation [in the manner of Tonon, (20)], and found that we could find power plant systems with overall plant Q in the range 4–5, an effective economic range.

We developed a relation for the centerpost gain. The widely used simple formula for fusion power [Eqs. (1) and (2) from Ref. (12)] agrees with tabulated values for σv at a temperature of about 30 keV. It overestimates the fusion power, compared to tables, by about 38% at 50 keV and underestimates the fusion power by about 30% at 10 keV. A more accurate treatment could be made in future work. We developed a formula for fusion power versus beta [Eq. (16)] by integrating over profiles. The profiles we used are characteristic of hot ion VH–mode and have a ratio of central pressure to volume average pressure of 3:1. Present day investigation of advanced tokamak physics suggests a pressure peaking of 5:1 may be optimal, in which case the fusion power produced would be greater than calculated herein. However, the specific equilibria being calculated to show the high beta potential of the ST have very broad pressure profiles and would produce lower fusion power (at the same beta) than is calculated herein. The integrations performed herein assume the ellipticity of the flux surfaces is a constant independent of radius; this assumption is not characteristic of most present peaked current profile equilibria but is characteristic of the broad and even hollow current profile equilibria (14) being developed to support very high beta in the ST. Such broad current profiles that substantially elongate the interior plasma flux surfaces have acquired a recent basis in experimental results in the negative central shear (NCS) regime in DIII–D (17). We have calculated the resistive dissipation in the centerpost neglecting the increase in resistivity with temperature. Because we found in Section IV that it is easy to provide sufficient cooling for the centerpost, it should be possible to design for a modest temperature rise that would limit the increase of the resistive power with temperature to perhaps 20%. Although we have discussed above a number of perturbations of the order of 20% to 40% to our calculations of the centerpost gain, we found in Eq. (26) a very strong size

dependence $\left(R_c^4\right)$ of the gain so that any shortfall in fusion power by a factor f or increase in centerpost dissipation by a factor f can be made up by an $f^{1/4}$ increase in the machine size. Accordingly, it is likely that the favorable view we have found for small devices with high gain will survive detailed design studies.

In Section IV, we found that the cooling of the centerpost imposes no meaningful restriction on the design of ST machines. Essentially because the water path is a short and once-through path, within the limits of acceptable water flow velocities (10 m/s), current densities in the very high range of 200 MA/m^2 could be supported. Such high current densities would lead to high toroidal field devices and fusion power outputs well in excess of what can be handled by blankets.

Apparently the high beta potential of the ST is so great that the physics of this device will not determine its size. Instead, the limit to neutron flux into the fusion blankets (Section V) was found to limit the size of the device. An aggressive assumption of 8 MW/m^2 at the blanket then leads to the small pilot plant and power plant possibilities that we have found. We examined the trade-off of elongation versus device size. We have chosen an elongation of 2.5 in our design cases. This elongation probably lies above the limit of passive vertical stability but below the limit of vertical stability using feedback. An increase of elongation from 2 to 3 can effect a factor of two reduction in the plasma (and so probably) the machine volume. Our considerations in this paper have treated elongation as an independent variable. Detailed stability calculations will undoubtedly develop the dependences $\kappa(A)$ and $\beta_N[\kappa(A])$ and incorporation of these relations into a formalism similar to this paper will lead to a different (probably lower) optimum value of aspect ratio than the value 1.4 that we have found.

We carried forward our analysis to a full plant model. We assumed there was enough design freedom in the outer legs of the toroidal coil and the upper and lower transitions from the centerpost to the outer TF coil legs to make the resistive dissipation in the outer legs 50% of the dissipation in the centerpost. We demanded a 90% bootstrap fraction,

according to the simple estimate $f_{bs} = \sqrt{\varepsilon}\,\beta_p$. This simple estimate is optimistic; calculatons in Eq. (14) suggest a coefficient of ~0.75 should be used, but the theory for bootstrap current at low *A* is evolving. We calculated the current drive power requirements for the various standard schemes to drive the remaining 10% of the current, assuming the current is driven where the temperature is the volume average temperature. We also evaluated helicity injection current drive, which is essentially edge current drive at the edge temperature. For the total current drive power, we took the average of the helicity injection (the largest power calculated) and the neutral beam current drive. We assigned various efficiency factors to relate the current drive power and resistive dissipation powers to the source electrical power. We assumed a blanket multiplication factor of 1.25 and that 50% of the electrical dissipation in various systems could be captured into the thermal cycle. With all these assumptions, we could then evaluate the net electric capability of the systems. We were able to find a pilot plant system with a plant Q = 1–2 and a small sized power plant system with a plant Q = 4–5.

Although more detailed system calculations should be done in the areas outlined above and for other aspects of the problem, the physics advances over today's database that are called for to make the ST path attractive involve a much greater reach than the level of inaccuracy in our approach to this assessment. Consequently the key next step in pursuit of the ST approach is to build some modest experiment capable of seeking to demonstrate the physics advances required. We briefly summarize the needed physics progress elements along the ST path.

1. High $\beta_N \sim 10$ at $A = 1.4$ and $\beta_T > 50\%$. The relation $\beta_N(A)$ must be determined first theoretically and then experimentally with the specific numerical goals above as targets.

2. High Elongation. The upper limits to $\kappa(A)$ must be established for both passive and feedback stabilized operation.

3. Confinement Database. Projections of present scalings to the low A regime are not useful.

4. Non-Inductive Startup. In order to build thermonuclear ST devices without an OH coil, an experimental demonstration of the non-inductive startup of a ~1 MA ST is needed.

5. Bootstrap Fraction and Alignment. Because the ST is inherently a high plasma current device, high bootstrap fraction is necessary.

6. Divertor Operation. The adequacy of divertor configurations that are achievable without a divertor coil and/or an inner leg must be explored.

7. Non-Inductive Current Drive. The low A regime without generally low B_T and high n_e poses specific challenges to find applicable current sustainment techniques.

8. Plasma Current Limitations. The lower bound on q(A) needs to be established experimentally.

VIII. CONCLUSIONS

In this paper, we find that within this ST concept, it appears (see Fig. 1) possible to design a pilot plant that would only be the size of the present DIII–D tokamak and yet still produce some net electric power. At double the size of the pilot plant we find full 1–2 GW net electric power plants with acceptable economics. The ST approach thus has the two key features of an executable commercialization strategy: a low cost pilot plant that can attract commercial cost sharing at an affordable level and with minimal financial risk, and a strong economy of scale leading to power plants that are still small on an absolute scale.

The pilot plant is the key to this strategy. With its small size, it offers a possibility to make net electric power for a total project cost under $1B. Commercial parties might be able to participate in such a project on a cost sharing basis with the government share still dominant . To justify any commercial participation, the device must be accepted by the commercial parties as a pilot plant. The most elementary definition of a pilot plant seems to be a device that makes electricity but does not necessarily sell any of it. In Table VIII, we have listed some other defining characteristics of a pilot plant and the way in which the ST matches up to these characteristics. Small size and cost are intrinsic to the ST concept. The small cost will enable cost sharing affordable to commercial parties. The power output is low, 50–200 MW net electric, rather than trying to initiate a new technology at the multi-gigawatt level. The device does not make a lot of net electric power. The plant Q, defined as the ratio of gross electric power to internal recirculating power is only 1–2, but remember that this pilot plant device does not have to sell electricity, just make some. The low plant Q will be acceptable in a pilot plant <u>if</u> the

Table VIII
Pilot Plant Characteristics

Desired Characteristic	ST Matchup
● Small size	≅ size of DIII–D
● Small cost	Follows from size and simplicity
● Small financial risk to investor	Able to attract cost sharing
● Small power output	50–250 MW(e)
● COE not important Plant Q ~ 1–2 acceptable	Q_{plant} ~ 1–2
IF	
● Strong economy of scale assured. Larger devices must make large power	$P_F/P_C \propto R_c^4$! Q_{plant} 4–6 possible P_{fusion} 3–5 GW
● All systems prototypical of full power plant. No new systems brought in at larger scale	True
● Simple, reliable	No inboard shield No OH system No inboard components except copper rod. Passively stable vertically – coils far away
● Can debug licensing process	Makes enough fusion power at low cost

concept has a strong economy of scale. The ST size scaling is very strong; the ratio of fusion power to the Ohmic dissipation in the copper TF coil magnet scales as the fourth power of the linear dimension. Consequently, we easily find small power plants with economically acceptable recirculating power (plant Q ~ 4–6, net electric power 1–2 GW). Another qualification of a pilot plant is that all of its systems must be prototypical of a full power plant. Commercial parties are interested in obtaining experience on operational reliability and complexity from their pilot plant participation and such experience loses much of its value if the technology of the system must be substantially

changed from the pilot plant to the power plant. The ST approach can progress from the pilot plant to the power plant just by doubling the linear dimensions of the device with no changes in technology. Indeed, we find that the physics and technical demands of this approach diminish with device size; the pilot plant machine is in many respects harder to develop than the power plants that would follow. Commercial parties also prize simplicity and the ST is a simplified tokamak with no hard to service inboard blankets, shields, PF or OH coils. Indeed, because the TF coil is copper, it can be jointed and so afford easy complete dissassembly of the machine for service. The ST concept offers high elongation and a natural divertor without a divertor coil. Finally, because that ST pilot plant is a full net electric and tritium producer, it will provide commercial parties with a full exercise of the siting and licensing process, but again at a low cost, low financial risk scale. The fact that a viable concept for a pilot plant exists is the principal attraction of the ST approach to government to commercial transition.

The development path afforded by the ST approach looks like what one expects of a commercial development path (Fig. 14); the number of devices at a given scale expands as time goes on. The ST path needs a small proof-of-principle device and a scale-up experiment to prove the reasonable but aggressive physics steps needed. The pilot plant could be built at the same size as the physics high performance device. After the demonstrations of the needed physics, the pilot plants would be seen to be so cost effective that probably two competing pilot plants (one in the U. S., one elsewhere) would be launched. Based on the pilot plant successes, even more demo scale plants would be built. This growing competitive environment is needed to produce the non-governmental sources of investment needed for the development of magnetic fusion energy.

IX. REFERENCES

1. Y-K. M. Peng and D. J. Strickler, "Features of Spherical Torus Plasmas," Nucl. Fusion **26**, 769, (1986)
2. Y-K. M. Peng and J. B. Hicks, "Engineering Feasibility of Tight Aspect Ratio Tokamak (Spherical Torus) Reactors," in the *Proceedings of the 16th Symposium on Fusion Technology*, London, September 3–7, 1990.
3. Y-K. M. Peng, et. al., "Summary of Workshop on Establishing the Physics Basis Needed to Access the Potential of Compact Toroidal Reactors," Fusion Technol. 1995.
4. A. C. Darke, et. al., "The Mega Amp Spherical Tokamak," in the *Proceedings of the 16th Symposium on Fusion Energy*, Champaign-Urbana, Illinois, 1995.
5. J. H. Chrzanowski, H. M. Fan, P. J. Heitzenroeder, M. Ono, J. Robinson, "Engineering Overview of the National Spherical Tokamak Experiment," *ibid*.
6. USTX reference.
7. A. Sykes, "Progress on Spherical Tokamaks," Plasma Phys. and Contr. Fusion **36**, B93 (1994).
8. A. Sykes, et. al., "The START Spherical Tokamak," Plasma Phys. and Contr. Nucl. Fusion Research **1**, 719, (1994).
9. T. R. Jarboe, et. al., "Formation and Sustainment of a Low Aspect Ratio Tokamak by Coaxial Helicity Injection," Plasma Phys. and Contr. Nucl. Fusion Research **1**, 725 (1994).
10. Y-K. M. Peng, et. al., "Physics Progress Towards Compact Tokamak Reactors with Normal Conducting Toroidal Field Coils," in the Proceedings of the 15th International Confercence on Plasma Physics and Controlled Nuclear Fusion

Research, Seville, Spain, 1994 (International Atomic Energy Agency, Vienna, 1995) Vol. 2, p. 643.

11. T.C. Hender, et. al., "Tight Aspect Ratio Tokamak Reactors," *ibid.*
12. *NRL Plasma Formulary* NRL/PU/6790-94-265, J. D. Huba, editor (1994).
13. J. D. Callen, B. A. Carreras, R. D. Stambaugh, "Stability and Transport Procession Tokamak Plasmas," Phys. Today **45**, 34 (1992).
14. R. L. Miller, Y. R. Lin-Liu, A. D. Turnbull, V. S. Chan, and L. D. Pearlstein, "Stability for Bootstrap-Current Driven Low Aspect Ratio Tokamaks," General Atomics Report GA-A22321, to be submitted to Phys. of Plasmas.
15. J. R. Ferron, L. L. Lao, T. S. Taylor, Y. B. Kim, E. J. Strait, D. Wróblewski, "Improved Confinement and Stability in the DIII–D Tokamak Obtained Through Modification of the Current Profile," Phys. Fluids B **5**, 2532 (1993).
16. R. D. Stambaugh, et al., "DIII–D Program Overview," Plasma Phys. and Contr. Nucl. Fusion Research **1**, 83 (1994).
17. E. A. Lazarus, et al., "Higher Fusion Power Gain With Pressure Profile Control in Strongly-Shaped DIII–D Tokamak Plasmas," General Atomics Report GA–A22292 (1996) submitted to Phys. Rev. Lett.
18. D. B. Montgomery, *Solenoid Magnet Design*, (Wiley-Interscience, New York, 1972).
19. R. D. Stambaugh, L. L. Lao, E. A. Lazarus, "Relation of Vertical Stability and Aspect Ratio in Tokamaks," Nucl. Fusion **32**, 1642 (1992).
20. G. Tonon, "Current Drive Efficiency Requirements for an Attractive Steady-State Reactor," in the Proc. of the Workshop on Tokamak Concept Improvement, Varenna, Italy, August 1994, p. 233.
21. P. N. Yushmanov, et al., "Scalings for Tokamak Energy Confinement," Nucl. Fusion **30**, 1999 (1990).

22. F. Ryter, et al., "Expression for the Thermal H–Mode Energy Confinement Time Under ELM-Free Conditions in Deuterium," Nucl. Fusion **33**, 979 (1993).
23. G. H. Miley, H. Towner, N. Ivich, "Fusion Cross Sections and Reactivities," University of Illinois Report COO-2218-17, June 1994.